



1 **Debris flow modeling at Meretschibach and Bondasca catchment,**  
2 **Switzerland: sensitivity testing of field data-based erosion model**

3 Florian Frank<sup>1</sup>, Brian W. McArdell<sup>1</sup>, Nicole Oggier<sup>2</sup>, Patrick Baer<sup>3</sup>, Marc Christen<sup>4</sup> and Andreas  
4 Vieli<sup>3</sup>

5 <sup>1</sup> Swiss Federal Institute for Forest, Snow and Landscape Research, Birmensdorf, 8903,  
6 Switzerland

7 <sup>2</sup> wasser/schnee/lawinen, Ingenieurbüro André Burkard AG, Brig-Glis, 3900, Switzerland

8 <sup>3</sup> Glaciology, Geomorphodynamics & Geochronology, Department of Geography, University of  
9 Zurich, Zurich, 8057, Switzerland

10 <sup>4</sup> WSL Institute for Snow and Avalanche Research SLF, Davos Dorf, 7260, Switzerland

11 *Correspondence to:* Florian Frank (florian.frank@wsl.ch)

12 **Abstract**

13 Debris flow volumes can increase due to the incorporation of sediment into the flow as a  
14 consequence of channel-bed erosion along the flow path. This study describes a sensitivity analysis  
15 of the recently-introduced RAMMS debris flow entrainment algorithm which is intended to help  
16 solve problems related to predicting the runout of debris flows. The entrainment algorithm predicts  
17 the depth and rate of erosion as a function of basal shear stress based on an analysis of erosion  
18 measurements at the Illgraben catchment, Switzerland (Frank et al., 2015). Starting with a  
19 landslide-type initiation in the RAMMS model, the volume of entrained sediment was calculated  
20 for recent well-documented debris-flow events at the Bondasca and the Meretschibach catchments,  
21 Switzerland. The sensitivity to the initial landslide volume was investigated by systematically  
22 varying the initial landslide volume and comparing the resulting debris-flow volume with estimates  
23 from the field sites. In both cases, the friction coefficients in the RAMMS runout model were  
24 calibrated using the model where the entrainment module was inactivated. The results indicate that  
25 the entrainment model predicts plausible erosion volumes in comparison with field data. By  
26 including bulking due to entrainment in runout models, more realistic runout patterns are predicted  
27 in comparison to starting the model with the entire debris-flow volume (initial landslide plus  
28 entrained sediment). In particular, lateral bank overflow – not observed during this event – is  
29 prevented when using the sediment entrainment model, even in very steep ( $\approx 60\text{--}65\%$ ) and narrow  
30 (4–6 m) torrent channels. Predicted sediment entrainment volumes are sensitive to the initial  
31 landslide volume, suggesting that the model may be useful for both reconstruction of historical  
32 events as well as the modeling of scenarios as part of a hazard analysis.



## 33 1. Introduction

34 Sediment erosion caused by debris flows strongly influences the bulking behavior of debris-flows  
35 (Iverson, 1997). The entrainment of sediment along the channel has been observed to considerably  
36 increase the volume of debris flows at many different locations (e.g. Hungr et al., 2005; Scheuner  
37 et al., 2009; Iverson et al., 2010; Berger et al., 2010a; Berger et al., 2011; Schürch et al., 2011;  
38 Iverson et al., 2011, McCoy et al., 2012; Tobler et al., 2014; Frank et al., 2015). Two recent  
39 extreme examples from the central Swiss Alps in the last decade showed significant bulking along  
40 the flow path. In the Spreitgraben catchment (2009-2011), the overall multi-surge event volumes  
41 increased to about 90'000 to 130'000 m<sup>3</sup> – mainly due to erosion along the active channel on the  
42 fan (Tobler et al., 2014; Frank et al., 2015). At the Rotlauigraben catchment (2005), about 2/3 of  
43 the total volume of 550'000 m<sup>3</sup> was eroded from the debris-flow fan during a multiple-surge  
44 debris-flow event initiated by the failure of a glacier moraine during an intense rainfall event  
45 (Scheuner et al., 2009). Therefore, the debris-flow erosion and bulking process should be included  
46 in debris-flow runout models to increase the accuracy of runout predictions including the overall  
47 runout distance, location and amplitude of lateral bank overflow but also – importantly for hazard  
48 assessment – the flow and depositional pattern on the fan (Gamma, 2000; Scheuner et al., 2009;  
49 Hussin et al, 2012; Han et al., 2015; Frank et al., 2015).

50 However, models which include bulking by debris flows are relatively new and their performance  
51 for practical applications has not yet been systematically investigated. Most entrainment modeling  
52 studies focused on the field site where the erosion data for the underlying entrainment modeling  
53 concept was collected and/or exclusively dealt with a single model application field site to test their  
54 concept for entrainment modeling (e.g. Han et al., 2015; Frank et al., 2015). Herein we describe the  
55 systematic application of the new RAMMS entrainment/bulking model (Frank et al., 2015) for  
56 several recent events in the Swiss Alps.

57 Computational debris-flow runout models, which usually neglect erosion, are often used to assess  
58 runout distance and pattern (Crosta et al., 2003; D'Ambrosio et al., 2003; Medina et al., 2008;  
59 Hungr and McDougall, 2009; Christen et al., 2012) and are therefore useful for hazard analysis  
60 where predictions of flow intensity (e.g. the spatial distribution of flow depth and velocity) are  
61 required (e.g. Scheuner et al., 2011). Because the debris flow process often was observed to cause  
62 significant entrainment of sediment which can strongly influence the flow (e.g. Dietrich and  
63 Dunne, 1978; Suwa and Okuda, 1980; Gallino and Pierson, 1984; Hungr et al., 1984; Benda, 1990;  
64 Pierson et al., 1990; Meyer and Wells, 1997; Vallance and Scott, 1997; Berti et al., 1999; Cannon  
65 and Reneau, 2000; Fannin and Wise, 2001; May, 2002; Wang et al., 2003; Revellino et al., 2004;  
66 Scott et al., 2005; Godt and Coe, 2007; Breien et al., 2008; Gartner et al., 2008; Guthrie et al.,  
67 2010; Procter et al., 2010; Berger et al., 2010; Berger et al., 2011; Schürch et al., 2011; Iverson et  
68 al., 2011; McCoy et al., 2012; Tobler et al., 2014; Frank et al., 2015), the importance of including  
69 entrainment and bulking debris flow runout modeling would be appropriate. Processed-based



70 entrainment rates using algorithms which consider the material properties of the debris flow bulk  
71 (Crosta et al., 2003; D'Ambrosio et al., 2003; Medina et al., 2008; Deubelbeiss and McArdeell,  
72 2012) as well as pre-specified entrainment rates which pre-define the absolute volume of eroded  
73 material (Beguería et al., 2009; Hungr and McDougall, 2009; Hussin et al., 2012) have been  
74 introduced in numerical runout **models**.  
75 Recently, we introduced an erosion algorithm in the RAMMS debris flow runout model for the  
76 assessment of debris flow **erosion** and **bulking** (Frank et al., 2015). The **erosion** algorithm uses a  
77 relation between basal shear stress and erosion based on an analysis of data from the Illgraben  
78 catchment, Switzerland (Frank et al., 2015; Berger et al., 2011; Schürch et al., 2011). The  
79 **entrainment** model was used to predict the overall **erosion** pattern and erosion volume at the first  
80 site where it was tested, the Spreitgraben, Switzerland. However, secondary erosion processes such  
81 as bank collapse and small torrential flood events between the debris flow events increased the  
82 uncertainty in the evaluation of the model. As a consequence, additional sensitivity tests were not  
83 made. In this study we therefore focus on testing the sensitivity of the RAMMS debris flow and  
84 entrainment model by assessing the sensitivity of total event volume (initial landslide volume plus  
85 volume of eroded sediment) to initial flow volume. This is especially important in hazard analysis  
86 where landslide scenarios are considered to trigger debris flows. For this sensitivity analysis, we  
87 evaluated two Alpine catchments with diverse topography and recent well-documented debris  
88 flows with volumes up to a few 10,000 m<sup>3</sup>: the Bondasca catchment in Southeastern Switzerland  
89 and the Meretschibach catchment in Southern Switzerland.

## 90 **2. Erosion modeling study sites and available data**

### 91 **2.1. Meretschibach catchment, Switzerland**

92 The Meretschibach catchment is located in Southern Switzerland, adjacent to and east of the  
93 Illgraben catchment (Figure 1). The catchment area is about 9.2 km<sup>2</sup> and ranges from the summit of  
94 the Bella Tola mountain (3,025 m a.s.l.) to the confluence with a drainage channel (619 m a.s.l.)  
95 following into the Rhone River. Debris flows in the Meretschibach currently originate mainly in  
96 the Bochtür subcatchment (1.42 km<sup>2</sup> area) which is covered mostly by steep debris slopes with  
97 hillslope angles on the talus deposits of up to 60%. Patches of forest are present below the treeline  
98 (2,200 m a.s.l.) and at the margins of the catchment, and largely contiguous forest is found along  
99 both sides of the channel below an elevation of 1,600 m. The Bochtür subcatchment is underlain by  
100 Triassic sericitized quartzite and white quartzites of the Bruneggjoch formation (Gabus et al. 2008).  
101 The surface has several terrace-like structures have been mapped as sacking-type features (Gabus  
102 et al., 2008) and are likely sources of landslides and rockfall.  
103 Sediment deposits are abundant on the steep slopes of the catchment, originating from a variety of  
104 mass wasting processes. Field observations of rockfall, the presence of damaged trees, and



105 unpublished records in the community forestry archives records indicate that rockfall is a dominant  
106 process for generating sediment. Observations in the source area also indicate that dry ravel of  
107 gravel and sand is also common in the summer months when the hillslopes are relatively dry.  
108 According to the event inventory debris flows occur mainly between April and October (Szymczak  
109 et al. 2010). Small debris flows start and deposit in the upper catchment, often depositing at an area  
110 of lower slope located an elevation of approximately 2,000 m a.s.l. Convective storms or long  
111 duration rainfall events have been observed to mobilize these sediment deposits and initiate debris  
112 flows.

113 Georadar profiles on the west side of the unforested part of the Bochtür subcatchment as well a  
114 airborne georadar measurements indicate that the sediment deposits are up to 5 m thick  
115 (Fankhauser et al., 2015), although independent observations of the spatial distribution of sediment  
116 thickness are not available. However extrapolation of that value to other parts of the catchment  
117 must be made with caution because the profiles were made on a talus deposit, which may be  
118 interpreted as a depositional area on the hillslope, that exhibits little geomorphic evidence of  
119 debris-flow activity.

120 In the years 2013 and 2014 several instruments and devices were installed in the catchment. In  
121 October 2013, a meteorological station was installed above the initiation zone to measure  
122 precipitation, temperature and snow height. Inexpensive wildlife-observation cameras recorded  
123 images every 15 minutes during daylight were positioned along the most active western channel to  
124 document the changes along the active channel. A debris flow monitoring station was installed on  
125 23 July 2014 (Oggier et al. 2015a). It consisted of three geophones and a radar to measure the flow  
126 stage. The radar is triggered by the geophones or the meteorological station and provides detailed  
127 recordings of the debris flow hydrograph at a resolution of 1 Hz.

128 During summer 2014, three debris flows occurred. Because the monitoring station was installed  
129 after the first event (20 July 2014), no hydrograph data are available for this event. Precipitation  
130 and hydrograph data for the debris flow events on 28 and 29 July 2014 indicate that the debris flow  
131 event on 28 July was triggered due to convective storms with large rainfall intensity (up to 3.3 mm  
132 / 10 min) while the event 29 July 2014 initiated after a few hours of steady rainfall with moderate  
133 intensity (up to 1.5 mm / 10 min). The pictures from camera 4 (see Fig. 1 for the location) clearly  
134 showed that the initiation of the event on July 28 took place between 19:45 and 20:15 (UTC +2),  
135 corresponding with the hydrograph measured at the observation station.

136 To obtain additional information about the initial volume and the spatial distribution of erosion, the  
137 height models from 15 July and 28 October were compared. The digital elevation model of 17 July  
138 was the result of a photogrammetry flight by swisstopo. The second digital elevation model (28  
139 October) – which is a surface model (including vegetation) – was taken with a drone (Oggier et al.  
140 2015b). The results indicate that the volume of the events eroded at the open debris slopes of



141 Bochtür was between 800 and 1,200 m<sup>3</sup>. Due to additional erosion downslope of the Bochtür  
142 subcatchment, the total volume of the debris flow events was between 8,000 and 10,000 m<sup>3</sup>.

## 143 **2.2. Bondasca catchment, Switzerland**

144 The Bondasca catchment in south-eastern Switzerland is a tributary to the Bergell valley (Figure 2).  
145 The catchment area covers about 20.9 km<sup>2</sup>. The geology is dominated by the Tertiary intrusion of  
146 the Bergell granite. Originating from within the North wall of Pizzo Cengalo, a rock avalanche on  
147 27 December 2011 deposited about 1.5 10<sup>6</sup> m<sup>3</sup> of sediments in the upper catchment with a runout  
148 of up to two kilometers from the rock wall. The deposits are up to 17 m thick and cover an area of  
149 about 0.760 km<sup>2</sup> while the hydrological sub-catchment is about 1.18 km<sup>2</sup> defined by the point  
150 where the channel leaves the rock avalanche deposits at the lower end of the deposit.

151 The sudden sediment input from the rock avalanche was followed by several debris flows in the  
152 summer of 2012 (5 and 14 July, 25 August, 24 September) whereof the two events in July  
153 evacuated about 90'000 m<sup>3</sup> of sediments from the rock avalanche deposit. The debris flows  
154 originated mainly just below a flat-shaped rock face. Some of the debris flow surges are thought to  
155 have been triggered due to water accumulation at the toe of the wall causing firehose-type debris  
156 flow initiation (Figure 3B and 5B) e.g. as described by Godt and Coe (2007). The slope of the  
157 channel on the rock avalanche deposit varies between approx. 32° (≈ 71 %) below the flat-shaped  
158 rock face and regularly decreases to 15° (≈ 33 %) at the lower end of the rock avalanche deposit.

## 159 **3. Debris-flow entrainment modeling**

160 The goal of this study is to evaluate the erosion algorithm implemented in the RAMMS debris flow  
161 model (version 1.6.25) which has been previously described by Frank et al. (2015). In particular,  
162 the sensitivity of the predicted erosion to the input parameters will be investigated, and the data sets  
163 described above provide a new basis for evaluating the model. The previous study (Frank et al.,  
164 2015) focused on demonstrating that more realistic runout results can be achieved when including  
165 sediment **entrainment and bulking** into the runout model. However that study also left many  
166 unanswered questions regarding the sensitivity of the model to input parameters, especially the  
167 initial landslide volume, which was not possible to assess in the previous study. Herein we focus on  
168 describing the sensitivity of the model to the initial landslide volume, using the two well-  
169 documented events described earlier in the paper.

170 Although the RAMMS model and the erosion algorithm have been published elsewhere, they will  
171 be briefly described below to provide the necessary background information for understanding the  
172 model. The underlying numerical formulas of shallow water equation and the Voellmy friction  
173 approach used in the RAMMS debris flow model are presented in detail in Christen et al. (2010);  
174 the field-data based empirical entrainment model is described in Frank et al. (2015).



### 175 **3.1. Computational debris-flow model RAMMS**

176 The RAMMS debris-flow model is based on 2D depth-averaged shallow water equations for  
177 granular flows in three dimensions given by the coordinates of the topographic surface of the  
178 digital elevation model in a Cartesian coordinate system  $(x, y, z)$  and at time  $(t)$  (Bartelt et al.,  
179 1999; Christen et al., 2010). The mass balance equation incorporates the field variables flow height  
180  $H(x, y, t)$  and flow velocity  $U(x, y, t)$  and is given by

$$181 \quad \dot{Q}(x, y, t) = \partial_t H + \partial_x(HU_x) + \partial_y(HU_y). \quad (1)$$

182 where  $\dot{Q}(x, y, t)$  describes the mass production source term and  $U_x$  and  $U_y$  represent the depth-  
183 averaged velocities in horizontal directions  $x$  and  $y$  (Christen et al., 2010). The depth-averaged  
184 momentum balance equations account for the conservation of momentum in two directions  $x$  and  $y$ :

$$185 \quad S_{g_x} - S_{f_x} = \partial_t(HU_x) + \partial_x\left(c_x HU_x^2 + g_z k_{a/p} \frac{H^2}{2}\right) + \partial_y(HU_x U_y), \quad (2)$$

$$186 \quad S_{g_y} - S_{f_y} = \partial_t(HU_y) + \partial_x(HU_x U_y) + \partial_y\left(c_y HU_y^2 + g_z k_{a/p} \frac{H^2}{2}\right). \quad (3)$$

187 where the earth pressure coefficient  $k_{a/p}$  is normally set to 1 when running the standard Voellmy-  
188 Salm friction approach,  $c_x$  and  $c_y$  represent topographical coefficients determined from the digital  
189 elevation model,  $S_g$  is the effective gravitational acceleration, and  $S_f$  the frictional deceleration in  
190 directions  $x$  and  $y$  (Christen et al., 2010). The frictional deceleration  $S_f$  of the flow is determined  
191 using the Voellmy friction relation (Salm et al., 1990, and Salm, 1993) and specifies the Coulomb  
192 friction  $\mu$  scaling with the normal stress and the **turbulent friction  $\xi$  depending on the velocity**  
193 squared (Christen et al., 2012; Bartelt et al., 2013):

$$194 \quad S_f = \mu \cdot \rho \cdot H g \cos(\phi) + \frac{\rho g U^2}{\xi} \quad (4)$$

195 where  $\rho$  is the mass density,  $g$  is the gravitational acceleration,  $\phi$  is the slope angle (approximately  
196 similar to the internal friction angle of the material), and  $H g \cos(\phi)$  is the normal stress on the  
197 overflowed surface. The tangent of the effective internal friction angle of the flow material can be  
198 defined for the resistance of the solid phase (the term containing  $\mu$ ) which extensively controls  
199 deceleration behavior of a slower moving flow. On the other hand, the resistance of the viscous or  
200 turbulent fluid phase (the term including  $\xi$ ) prevails for a quicker moving flow (Bartelt et al.,  
201 2013).



### 202 3.2. Debris-flow entrainment model

203 The entrainment model was constructed using field data from the Illgraben catchment in  
204 Switzerland (Frank et al., 2015). The entrainment model describes the maximum erosion depth as a  
205 function of channel-bed shear stress and the vertical erosion rate of channel-bed sediment erosion.  
206 In detail, the model is based on the analysis of differential elevation models from pre- and post-  
207 event DTMs by Schürch et al. (2011b). This provides the depth of net erosion in a cell as a function  
208 of the local shear stress acting on the channel bed at the base of the flow. Similarly, the rate of  
209 erosion is constrained to be at the rate reported by Berger et al., 2011, using *in situ* erosion sensors,  
210 also at the Illgraben channel. In the analysis of Schürch et al (2011b), flow heights were determined  
211 using values interpolated between lateral levees after each event and the shear stress  $\tau$  is  
212 approximated using the depth-slope product:

$$213 \quad \tau = \rho g h S \quad (5)$$

214 where  $\rho$  is the bulk mass density of the flow,  $h$  is flow height, and  $S$  is the channel slope. An  
215 approximation of the typical potential erosion depth at the Illgraben follows the 50% percentile line  
216 fit to the distribution of elevation change for four debris flow events (Fig. 3a in Schürch et al.,  
217 2011b). The erosion algorithm implemented in the RAMMS entrainment model is defined by the  
218 maximum potential erosion depth  $e_m$  and a specific erosion rate. The relationship between the shear  
219 stress estimated and the measured erosion (Schürch et al., 2011b) is described as a linear function  
220 of shear stress using a proportionality factor  $\frac{dz}{d\tau}$  (Eq. 2). The maximum potential erosion depth  $e_m$  is  
221 calculated using a critical shear stress  $\tau_c (= 1 \text{ kPa})$  and the proportionality factor  $\frac{dz}{d\tau} (= 0.1 \text{ m kPa}^{-1})$   
222 as a function of basal shear stress  $\tau$ :

$$223 \quad e_m = \begin{cases} 0 & \text{for } \tau < \tau_c \\ \frac{dz}{d\tau} (\tau - \tau_c) & \text{for } \tau \geq \tau_c \end{cases} \quad (6)$$

224 The average rate of erosion recorded at the erosion sensor site during the Illgraben debris flow  
225 event of 1 July 2008 (Berger et al., 2011) is used to define a specific erosion rate  $\frac{dz}{dt}$ .

$$226 \quad \frac{dz}{dt} = -0.025 \text{ for } e_t \leq e_m \quad (7)$$

227 When the critical shear stress  $\tau_c$  is exceeded, sediment can be entrained from the channel.  
228 Entrainment stops when the actual erosion depth  $e_t$  reaches the maximum potential erosion depth  
229  $e_m$  (Eq. 2). Normally, the specific erosion rate is implemented using the default value  $\frac{dz}{dt} =$   
230  $-0.025 \text{ ms}^{-1}$  (Eq. 3) as presented in Frank et al. (2015). However, the model also allows to



231 account for larger or smaller erosion scenarios by either doubling the rate or cutting it in half. In  
232 this study, we will use these variable erosion rates for testing the sensitivity of the model.

### 233 **3.3. Erosion model setup**

#### 234 **3.3.1. Topographic resolution**

235 This study focuses on the evaluation of the sensitivity of the predicted (modeled) channel-bed  
236 erosion in relation to the initial volume (e.g. initial landslide size) and the comparison of the model  
237 results and the erosion pattern observed in the field. The ability to reproduce the observed erosion  
238 patterns highly depends on a realistic representation of the channel morphology where the channel  
239 is clearly visible in the DTM (Deubelbeiss et al., 2010 and 2011; Scheuner et al., 2011; Hohermuth  
240 and Graf, 2014) and the channel dimensions (e.g. cross-sectional area) in the DTM have to be  
241 similar to what is observed in the field (e.g. Frank et al., 2015). In this study, the initial topographic  
242 data available for the Meretschibach catchment (described above) are on a square grid of 0.5 m for  
243 a channel with a width of 2 to 4 m. At the Bondasca catchment data are available on a 2 m square  
244 grid for channel varying in width from about 5 to 20 m. Although a channel width to DTM grid  
245 spacing ratio of more than 5 to 10 would probably produce more accurate results, such data are  
246 generally unavailable and the increase in the time for a simulation would be impractical.

#### 247 **3.3.2. Erosion model starting condition: block release and input hydrograph**

248 The type of initial release mechanism, lock release or input hydrograph, can be determined based  
249 on field observations, potential model constraints and previous modeling experience using the  
250 RAMMS debris flow model (Bartelt et al., 2013). Recent debris flow modeling studies  
251 (Deubelbeiss et al., 2010; Deubelbeiss et al., 2011; Han et al., 2015) summarized that debris flows  
252 in steep channels are mostly triggered by the sudden destabilization of material originating from  
253 lateral bank collapses or dam-type deposits located within the channel itself. Han et al. (2015)  
254 concluded that a hypothetical scenario such as the breaking of a dam – which they used to start  
255 their erosion model simulations – provides a stable and consistent release method. Deubelbeiss et  
256 al. (2010 and 2011), for a case study in the Swiss Alps, suggested that the block release method is  
257 most appropriate method for small to moderate initial volumes ranging from  $1 \text{ m}^3$  up to  $100 \text{ m}^3$   
258 using the RAMMS debris flow model. The alternative release method using a discharge  
259 hydrograph seems to be more suitable for larger initial volumes (Deubelbeiss et al., 2010 and 2011)  
260 ( $> 100 \text{ m}^3$ ) which – in general – might be plausible for the larger channel of the Bondasca  
261 catchment.

262 The main problem with the block release is that the initial flow depth, width, or length of the initial  
263 landslide can be unrealistically large in comparison to field observations. Users have to resort to  
264 such large initial landslide volumes because most models do not allow for erosion along the





265 channel path. The total debris flow volume, typically measured in the deposition zone, is often used  
266 as the initial landslide volume, thereby implicitly ignoring the possibility that channel-bed erosion  
267 and flow bulking occur (Frank et al., 2015). The input hydrograph starting condition in RAMMS  
268 was intended to help circumvent this problem by allowing users to specify an influx of debris as a  
269 function of time at a point lower in the watershed (e.g. just above the fan apex).  
270 The block release volume is calculated by defining a specific block release height (with a precision  
271 of 1 cm) based on a pre-defined release area. The model assumes an instantaneous failure of the  
272 landslide. The initial landslide surface elevation is then set to the initial elevation of the land  
273 surface using an automatic procedure in RAMMS (the “subtract release from DTM” option in  
274 RAMMS introduced in version 1.6.45). The main advantage of this procedure is that it prevents  
275 unrealistic lateral spreading of the initial landslide mass in comparison with a landslide “block”  
276 situated on top of the land surface.

### 277 3.3.3. Specified erosion rates

278 As a basis for comparison of the sensitivity of the erosion algorithm, we hold constant the default  
279 erosion model coefficients (critical shear stress  $\tau_c$ , potential erosion depth as a function of basal  
280 shear stress  $\frac{dz}{dt}$ , erosion rate  $\frac{dz}{dt}$ ) described above. In the previous study (Frank et al., 2015) we  
281 demonstrated that an erosion rate of  $\frac{dz}{dt} = 2.5$  cm s<sup>-1</sup> based on field data from the Illgraben  
282 catchment, Switzerland (Berger et al., 2011) produces plausible results for the much steeper  
283 Spreitgraben catchment. The catchments described in this paper are different in size and slope, so  
284 one might expect some variation in erosion rate. However, the erosion algorithm in RAMMS  
285 allows for rates up to  $\frac{dz}{dt} = 5.0$  cm s<sup>-1</sup>, with an option to include a shape file describing where  
286 erosion may occur e.g. to account for engineering structures such as check dams or sills, or natural  
287 features such as bedrock, where significant erosion is not expected during one debris-flow event.  
288 For comparison we also used a rate of  $\frac{dz}{dt} = 1.25$  cm s<sup>-1</sup> based on a lower rate from Berger et al.  
289 (2011).

## 290 4. Erosion and entrainment: observations and modeling results

### 291 4.1. Erosion patterns and entrainment model calibration

292 The observed erosion patterns are the basis for calibrating the RAMMS model coefficients, in  
293 particular the friction coefficients  $\xi$  and  $\mu$  are systematically adjusted in successive model runs,  
294 until a satisfactory model result is achieved. The erosion pattern is derived by assessing the  
295 difference between the digital elevation models. In both study areas, a measured erosion pattern  
296 caused by one single debris flow event is not available. We therefore focus on the spatial



297 distribution of erosion and deposition, instead of attempting to exactly predict the spatial change  
298 due to the debris flow process.

299 In the Meretschibach, the change in the DTM includes the erosion due to three debris flow events  
300 which appear to have originated on an open-slope talus deposit (Figure 3A). The location of the  
301 release area at the Meretschibach corresponds to the upper most visible erosion scar visible in the  
302 DTM analysis and as described above includes the erosion due to three debris flow events between  
303 July 17 to October 28, 2014 (Fig. 3A). Therefore, the release area was placed within the channel,  
304 where up to 2.5 meters of erosion was observed (upper end of the blue polygon at about 1750 m  
305 a.s.l. in Fig. 3A.). The location is just below a bedrock step intersecting the main channel at about  
306 1800 m a.s.l. Further monitoring at the upper Bochtür subcatchment using interval cameras and  
307 conducting field observations on the site itself confirmed that at least some of the debris flows most  
308 likely initiated at this location.

309 We calibrated the RAMMS model using an initial block release volume of  $10 \text{ m}^3$  which  
310 corresponds to the channel depth of 1-2 m and a width of 2-4 m at this location. To keep the initial  
311 volume within the channel and prevent unrealistic lateral outflow, no-flux boundaries were created  
312 at the lateral sides of the initial landslide block. Within the middle and lower channel sections (Fig.  
313 3A, blue polygon), the observed runout and relative erosion patterns can be best reproduced using  
314 Voellmy friction parameters  $\xi = 200 \text{ ms}^{-2}$  and  $\mu = 0.6$  (Fig. 3B2). The modeled velocities of  
315  $6\text{-}9 \text{ ms}^{-1}$  using  $\xi = 200$  are plausible, although independent field data are not available for  
316 comparison. The parameter combination  $\xi = 200 \text{ ms}^{-2}$  and  $\mu = 0.7$  results in overbank flow along  
317 both sides of the middle channel, which was not observed in the field (Fig. 3C2). There were  
318 neither deposits outside of the channel nor were levees deposited along this entire channel reach  
319 (Fig. 3A, blue polygon). In contrast, the erosion pattern using  $\xi = 200 \text{ ms}^{-2}$  and  $\mu = 0.5$  resulted in  
320 an even distribution of erosion along the entire channel length, which is inconsistent with the field  
321 results which showed locations of deeper erosion depths (Fig. 3A). Within the normal range of the  
322  $\xi$  parameter (Bartelt et al., 2013) the differences in flow and erosion patterns were small in  
323 comparison to those resulting from variations in  $\mu$ , and are therefore not described herein. Hence,  
324 the further model runs were conducted using the best-fit parameters  $\xi = 200 \text{ ms}^{-2}$  and  $\mu = 0.6$  in the  
325 sensitivity analyses described in subsequent sections.

326 In the Bondasca catchment, the differential elevation model includes both the rock avalanche  
327 deposit (27 December 2011) and the erosion due to one debris-flow event (5 July 5, 2012) (Fig. 5).  
328 The upper end of channel erosion is located just below a planar outcrop of bedrock (Fig. 4B)  
329 corresponding to the likely location debris flow initiation zone (Fig. 5C). The surface runoff  
330 channels along the west side of the wall and runoff across the wall surface (Fig. 4B) converge on  
331 the sediments at the bottom of the rock wall (see pictures from 2014 in Fig. 5). This scenario  
332 suggests a firehose-type debris-flow initiation (e.g. Godt and Coe, 2007). Hence, this location was  
333 used for the runout modeling.



334 The observed erosion along the main debris flow channel (Fig. 5C) – resulting from the two debris  
335 flow events in July 2012 – were used to calibrate the RAMMS model within the upper two thirds of  
336 the study reach (Figure 4B, brown polygon) by varying the model parameters  $\xi$  and  $\mu$ . The best fit  
337 was found with the parameter combination  $\xi = 400 \text{ ms}^{-2}$  and  $\mu = 0.3$ . However, the observed  
338 elevation change also includes secondary processes such as lateral bank collapse and the deposits  
339 of debris-flow snouts and levees within the channel. Channel sections where the events eroded into  
340 the deposits present can also be identified by the stratigraphy in the field.

#### 341 **4.2. Entrainment modeling and runout patterns**

342 The runout of a (landslide-type) block release of  $10 \text{ m}^3$ , neglecting erosion (Fig. 6A) results in  
343 maximum flow heights smaller than 0.5 m and the flow stops in the channel upstream of the  
344 deposition zone. By contrast, including debris-flow erosion (Fig. 6B) leads to a more realistic flow  
345 pattern consisting of flow within the channel reaching the deposition zone without any lateral  
346 outflow. For comparison, if the total event volume ( $\approx 1,555 \text{ m}^3$ ) is released as a landslide and the  
347 debris-flow is not allowed to erode the channel (Fig. 6C), the runout shows overbank flow along  
348 the upper channel reaches below the initiation area. The last scenario is a typical example of how  
349 debris-flow runout models are used when the total event volume is known. These results illustrate  
350 the ability of the runout model to better predict the erosion pattern if the channel-bed erosion and  
351 bulking process is included in the model.

#### 352 **4.3. Erosion model sensitivity testing**

353 The results show that the total volume of eroded sediment, at both field sites, depends strongly on  
354 the initial landslide volume. At both the Meretschibach and the Bondasca catchments, there is a  
355 strong increase in the amount of sediment entrained and consequent increase in debris-flow volume  
356 (Fig. 7) for relatively small increases of the initial landslide volume. At the Meretschibach  
357 catchment, the erosion model – using the default maximum erosion rate  $\frac{dz}{dt} = 2.5 \text{ cm s}^{-1}$  – shows the  
358 highest sensitivity to the total erosion volume between 2 and  $3 \text{ m}^3$  of initial block release (e.g.  
359 initial landslide volume). Above  $4\text{-}5 \text{ m}^3$  of initial block volume the increase of the total erosion  
360 volume within the erosion domain remains approximately constant. The cause for the rapid  
361 increase is related to the critical shear stress in the entrainment algorithm. Small initial landslides  
362 do not generate enough shear stress to initiate erosion, whereas larger landslides can cause erosion  
363 over the entire computational domain.

364 If we double the erosion rate to  $\frac{dz}{dt} = 5.0 \text{ cm s}^{-1}$  based on field estimates reported by Frank et al.,  
365 2015 for the Spreitgraben catchment, a similar pattern is observed in the relationship between total  
366 erosion volume as a function of initial release volume. However the erosion volumes are 3 to 5  
367 times larger than the ones resulting from the default erosion rate at the same initial release volume.



368 In contrast, implementing only half the default maximum erosion rate ( $\frac{dz}{dt} = 1.25 \text{ cm s}^{-1}$ ) for low  
369 erosion scenarios decreases the sensitivity to initial volume in an analogous manner.  
370 Similar trends in total erosion volume as a function of initial block release (landslide) volume are  
371 observed at the Bondasca catchment. However, the model only starts to predict significant erosion  
372 volumes for block releases exceeding  $20 \text{ m}^3$ , and the progressive increase in total erosion volume  
373 as a function of initial block release volume is somewhat less steep. For the default erosion rate  $\frac{dz}{dt}$   
374  $= 2.5 \text{ cm s}^{-1}$  (Frank et al., 2015), total erosion volumes increase most strongly between initial  
375 volumes of  $20$  to  $100 \text{ m}^3$ . The topography at the Bondasca catchment is somewhat less steep and  
376 more variable, which may help explain these differences. Doubling the default erosion rate at the  
377 Bondasca catchment results in the onset of erosion for initial volumes between  $20$  and  $30 \text{ m}^3$ . When  
378 reducing the default erosion rate to half of the default value, the erosion model depicts a somewhat  
379 less sensitive reaction of the erosion model than using the default rate.

## 380 5. Discussion

381 The total erosion volumes observed in the sensitivity tests (Fig. 7) indicate a strong sensitivity to  
382 block release volume (initial landslide volume) over a relatively narrow range of block release  
383 volumes. This result is based on the assumption that the entire landslide fails instantaneously and  
384 not progressively as a sequence of smaller landslides over a longer period of time. Information on  
385 the style of initial landslide failure are not available for either field site, therefore we focus the  
386 discussion on other factors related to the runout modeling. One striking difference between the two  
387 field sites is that the size of the block release necessary to cause significant erosion is an order of  
388 magnitude larger at the Bondasca site. The channel cross-sectional area where the flow travels and  
389 therefore where the erosion model is active is different at the two field sites. The Meretschibach is  
390 substantially steeper ( $50$  to  $65\%$  vs.  $15$  to  $35\%$ ). This results in larger shear stresses at the  
391 Meretschibach for the same initial landslide thickness, because the shear-stress varies as the  
392 product of initial release thickness, flow density, and channel slope. Other factors such as  
393 differences in channel-bed roughness may also be important, however the Voellmy friction relation  
394 within RAMMS does not explicitly consider channel-bed roughness.

395 In the RAMMS debris flow model, the development of the flow properties is controlled by the  
396 Voellmy friction parameters  $\xi$  and  $\mu$  (described in section 3.1) where  $\xi$  is the dominant control over  
397 the flow velocities when the flow is moving rapidly and  $\mu$  controls the runout distance. The  $\xi$   
398 parameter was found in this study to have a relatively small influence over the flow behavior in  
399 comparison with the Coulomb friction term  $\mu$ . The RAMMS manual (Bartelt et al., 2013) suggests  
400 using the tangent of the fan slope as first estimate to determine  $\mu$ . As described in the calibration  
401 procedure (section 3.2), this corresponds to relative erosion patterns measured by differential DTM  
402 analysis. Hence, we conclude that the tangent of the channel slope can be used as a first approach



403 to define parameter  $\mu$  also for the erosion model, which was also found to be useful by Frank et al.  
404 (2015) in the first application of the model.  
405 Morphological effects influence the erosional behavior of the field data based erosion model. The  
406 Bondasca channel is more variable in width and planform direction compared to the comparably  
407 uniform and straight Meretschibach channel. This difference will cause larger spatial variability in  
408 shear stress at Bondasca channel and therefore the channel will have a more variable onset of  
409 debris flow erosion along the length of the channel. In the Bondasca catchment, the channel where  
410 erosion takes place is significantly wider (4-10 m) than in the Meretschibach (1-3 m). On the one  
411 hand, the flow can laterally spread more often in Bondasca than in the Meretschibach, thereby  
412 locally reducing flow height, shear stresses and maximum potential erosion depth. On the other  
413 hand, once the critical shear stress is exceeded, the potential erosion depth tends to increase more  
414 rapidly in a narrow channel such as in the Meretschibach channel.  
415 Another difference between the Meretschibach and the Bondasca channels is that the Bondasca  
416 channel bed has a rougher surface with more scours holes, and larger blocks within the channel  
417 which are similar in size to the nominal width of the channel. The model does not consider local  
418 variations in erodibility due to the presence of large blocks, so local scour patterns in the field  
419 around the large blocks are not present in the model results. Prancevic and Lamb, (2015a)  
420 suggested that in rough mountain channels the large particles can be interlocked and hence more  
421 stable. In contrast, local concentration of the flow between such large blocks may cause locally  
422 very large shear stresses and corresponding large erosion rates. However, we do not have enough  
423 information on the mobility of the large blocks, so this question cannot be addressed in more detail  
424 herein.  
425 The current version of the RAMMS model with erosion (version 1.6.45) does not adjust the  
426 elevation of the bed when erosion occurs. The erosion can be subtracted from the initial DTM as a  
427 post-processing step within the user interface, e.g. for modeling subsequent surges. This issue was  
428 discussed at length by Frank et al (2015), and it can potentially complicate the interpretation of  
429 erosion patterns resulting from multiple debris flows. Insufficient field data are available to help  
430 constrain the events described herein.  
431 Further assessment of the relation of the total erosion volumes depending on the initial volumes can  
432 be made by calculating a bulking factor. **The bulking factor BF** is the ratio between the total  
433 erosion volume  $V_{ero}$  to the initial volume  $V_{ini}$  :

$$434 \quad BF = V_{ero}/V_{ini} \quad (8)$$

435 At the Meretschibach channel, the bulking factor is  $\approx 200$  when the erosion model using the default  
436 erosion rate and an initial volume of  $3 \text{ m}^3$  (Fig. 8). The BF reaches a peak  $BF_p \approx 300$  at a release  
437 volume of  $4 \text{ m}^3$ . It then drops to a  $BF \approx 30$  for an initial volume of  $100 \text{ m}^3$ . The model simulations  
438 using the doubled default erosion rate show a bulking factor peak  $BF_p \approx 1,800$  for an initial release



439 volume of  $2 \text{ m}^3$ ; half the default erosion rate shifts this peak to  $50 \text{ m}^3$  for the initial volume but the  
440 corresponding peak bulking factor drops significantly down to  $\approx 14$ .

441 The behavior of the bulking factor for the default erosion rate at the Bondasca catchment is  
442 relatively smooth when compared to that at the Meretschibach. A peak bulking factor can be  
443 identified somewhere between 200 and  $500 \text{ m}^3$  but the value is lower in comparison ( $\approx 11$ ) for the  
444 default erosion rate. The doubled rate leads to a peak bulking factor  $\text{BF}_p$  of  $\approx 700$  at a release  
445 volume of  $30 \text{ m}^3$ . That is still large compared to examples in the literature (BF from 10 to 50  
446 reported by Berti et al., 1999 and Vandine and Bovis, 2002). Nevertheless, a several hundred fold  
447 increase of the debris flow volume due to bulking is plausible for extreme erosion cases. Larger  
448 erosion rates might be expected for pyroclastic deposits (not present in the catchments described  
449 herein) or due to the presence of very recent rock avalanche deposits which may contain firn-ice-  
450 debris mixtures (e.g. Spreitgraben, Tobler et al., 2014; Frank et al., 2015). Large erodibilities may  
451 be expected at the Bondasca catchment because the rock avalanche event occurred during winter  
452 and may have contained significant amount of snow.

453 Due to the very long ( $\approx 4 \text{ km}$ ) and flat ( $\approx 15\%$ ) channel section in the middle segment of the  
454 Bondasca catchment, the estimated deposition volumes ( $\approx 40,000 \text{ m}^3$ ) above the inlet of the  
455 Bondasca river in the central valley are highly influenced by further erosional and depositional  
456 processes along the channel.

## 457 6. Conclusion

458 Debris-flow runout predictions can be improved when considering the increase in flow volume  
459 along the flow path. Using a recently-introduced empirical erosion algorithm within the RAMMS  
460 2D runout model (Frank et al., 2015) we illustrate that runout patterns at the Meretschibach and  
461 Bondasca catchments, in Switzerland, can be accurately modeled. When calibrated with field data,  
462 the model produces more realistic runout patterns compared to simulations which do not consider  
463 entrainment and bulking. In particular, we could show that even in very steep ( $\approx 60\text{--}65\%$ ) and  
464 narrow (4–6 m) torrent channels, lateral overflow – not observed in the field case – is prevented  
465 when applying the entrainment model. However the model results can be quite sensitive to the  
466 volume of the initial block release in the model which corresponds to the initial landslide volume.  
467 The predicted erosion volumes are sensitive to the initial debris flow volume, with bulking factors  
468 approaching 2000 predicted by the model, depending on the scenario considered. However, the  
469 results are also sensitive to slope angle and channel morphology. The two field sites differ  
470 substantially: the Meretschibach catchment is very steep with a straight and narrow channel,  
471 whereas the Bondasca channel is less steep but morphologically more complex, yet the calibration  
472 procedure is the same as for the standard RAMMS model which does not include the entrainment  
473 process. The overall method presented herein is useful for case studies where sufficient data are



474 available to constrain the model results. However, more case studies have to be conducted to  
475 develop a more comprehensive recommendation for modeling the runout of erosive debris flows in  
476 natural terrain.

#### 477 **Acknowledgements**

478 This project was partially supported by the CCES-TRAMM project. We are grateful to Christian  
479 Huggel for helpful discussions and comments. We thank Martin Keiser of Amt für Wald und  
480 Naturgefahren of Canton Graubünden for providing elevation data for the Bondasca catchment and  
481 Ruedi Bösch, WSL, for the elevation data at the Meretschibach catchment.



## 482 **References**

- 483 Beguería, S., Van Asch, Th. W. J., Malet, J.-P., and Gröndahl, S.: A GIS-based numerical model  
484 for simulating the kinematics of mud and debris flows over complex terrain, *Nat. Hazards Earth*  
485 *Syst. Sci.*, 9, 1897–1909, doi:10.5194/nhess-9-1897-2009, 2009.
- 486 Bartelt, P., Buehler, Y., Christen, M., Deubelbeiss, Y., Graf, C., and McArdell, B. W.: RAMMS –  
487 rapid mass movement simulation, A modeling system for debris flows in research and practice,  
488 user manual v1.5, debris flow, manuscript update: 31 January 2013, WSL Institute for Snow  
489 and Avalanche Research SLF, available at:  
490 [http://ramms.slf.ch/ramms/downloads/RAMMS\\_DBF\\_Manual.pdf](http://ramms.slf.ch/ramms/downloads/RAMMS_DBF_Manual.pdf) (last access: 27 February  
491 2015), 2013.
- 492 Benda, L.: The influence of debris flows on channels and valley floors in the Oregon Coast Range,  
493 USA. *Earth Surf. Proc. Landf.* 15, 457-466, 1990.
- 494 Berger, C., McArdell, B.W., and Schlunegger, F.: Sediment transfer patterns at the Illgraben  
495 catchment, Switzerland: Implications for the time scales of debris flow activities,  
496 *Geomorphology*, 125, 421–432, 2010.
- 497 Berger, C., McArdell, B. W., and Schlunegger, F.: Direct measurement of channel erosion by  
498 debris flows, Illgraben, Switzerland, *J. Geophys. Res.*, 116, F01002,  
499 doi:10.1029/2010JF001722, 2011.
- 500 Berti, M.; Genevois, R.; Simoni, A. and Tecca, P.R.: Field observations of a debris flow event in  
501 the Dolomites. *Geomorphology*, 29:265–274, 1999.
- 502 Breien, H., De Blasio, F. V., Elverhøi, A & Høeg, K. Erosion and morphology of a debris flow  
503 caused by a glacial lake outburst flood, western Norway. *Landslides* 5, 271-280, 2008.
- 504 Cannon, S. H. and Reneau S. L.: Conditions for generation of fire-related debris flows, Capulin  
505 Canyon, New Mexico, *Earth Surf. Processes Landforms*, 25(10), 1103-1121, 2000.
- 506 Christen, M., Kowalski, J., and Bartelt, P.: RAMMS: Numerical simulation of dense snow  
507 avalanches in three-dimensional terrain, *Cold Reg. Sci. Technol.*, 63, 1–14, 2010.
- 508 Christen, M., Bühler, Y., Bartelt, P., Leine, R., Glover, J., Schweizer, A., Graf, C., McArdell, B.  
509 W., Gerber, W., Deubelbeiss, Y., Feistl, T., and Volkwein, A.: Integral hazard management  
510 using a unified software environment: numerical simulation tool “RAMMS” for gravitational  
511 natural hazards, edited by: Koboltschnig, G., Hübl, J., Braun, J., 12th Congress  
512 INTERPRAEVENT, 23–26 April 2012 Grenoble, France, Proceedings, Vol. 1, Klagenfurt,  
513 International Research Society INTERPRAEVENT, 77–86, 2012.
- 514 Crosta, G. B., Imposimato, S., and Roddeman, D. G.: Numerical modelling of large landslides  
515 stability and runout, *Nat. Hazards Earth Syst. Sci.*, 3, 523–538, doi:10.5194/nhess-3-523-2003,  
516 2003.





- 517 D'Ambrosio, D., Di Gregorio, S., and Iovine, G.: Simulating debris flows through a hexagonal  
518 cellular automata model: SCIDDICA S3-hex, Nat. Hazards Earth Syst. Sci., 3, 545–559,  
519 doi:10.5194/nhess-3-545-2003, 2003.
- 520 Deubelbeiss, Y.; Graf C.; McArdell, B.; Bartelt, P.: Numerical modeling of debris flows – Case  
521 study at Dorfbach, Randa (VS), Swiss Geoscience Meeting. Fribourg, 2010.
- 522 Deubelbeiss, Y.; Graf, C.; McArdell, B.; Bartelt, P. Numerical modeling of debris flows – Case  
523 study at Dorfbach, Randa (Valais, Switzerland). Geophysical Research Abstracts Vol. 13,  
524 EGU2011-5681, EGU General Assembly 2011, Vienna, 2011.
- 525 Deubelbeiss, Y. and McArdell, B. W.: Dynamic modelling of debris-flow erosion and deposition  
526 with application to the USGS debris flow flume experiments, Geophys. Res. Abstr. 14,  
527 EGU2012-7906, 2012.
- 528 Dietrich, W. E., and Dunne, T.: Sediment budget for a small catchment in mountainous terrain, *Z.*  
529 *Geomorphology*, 29, 191-206, 1978.
- 530 Fannin, R. J. and Wise, M. P.: An empirical\_statistical model for debris flow travel distance. *Can.*  
531 *Geotech. J.* 38, 982-994, 2001.
- 532 Fankhauser F., Lucas Guzman D. R. Oggier N., Maurer H., Springman S. M. 2015. Seasonal  
533 Response and Characterization of a Scree Slope and Active Debris Flow Catchment Using  
534 Multiple Geophysical Techniques: The case of the Meretschibach Catchment, Switzerland.  
535 Geophysical Research Abstracts Vol. 17, EGU2015-PREVIEW, EGU General Assembly 2015,  
536 2015.
- 537 Frank, F., McArdell, B. W., Huggel, C., and Vieli, A.: The importance of entrainment and bulking  
538 on debris flow runout modeling: examples from the Swiss Alps, Nat. Hazards Earth Syst. Sci.,  
539 15, 2569-2583, doi:10.5194/nhess-15-2569-2015, 2015.
- 540 Frank, F., McArdell, B. W., Huggel, C., and Vieli, A.: Sediment input and debris flow system  
541 activity cycles - an analysis of the development in different catchments in Switzerland. In prep.
- 542 Gabus, J. H., Weidmann, M., Bugnon, P.-C., Burri, M., Sartori, M., and Marthaler, M.: Geological  
543 map of Sierre, LK 1278, sheet 111, scale 1:25,000, in Geological Atlas of Switzerland, Swiss  
544 Geol. Surv., Bern, Switzerland, 2008.
- 545 Gallino, G. L., and Pierson, T. C.: The 1980 Polallie Creek debris flow and subsequent dam-break  
546 flood, East Fork Hood River Basin, Oregon, U.S. Geol. Surv. Open File Rep., 84-578, 37 pp.,  
547 1984.
- 548 Gamma, P.: "dfwalk" Ein Murgang-Simulationsmodell zur Gefahrenzonierung. Institute of  
549 Geography, University of Berne. Geographica Bernensia G66 (only available in German), 2000.
- 550 Gartner, J. E., Cannon, S. H., Santi, P. M. and Dewolfe, V. G.: Empirical models to predict the  
551 volumes of debris flows generated by recently burned basins in the western U.S.,  
552 *Geomorphology*, 96(3-4), 339-354, 2008.



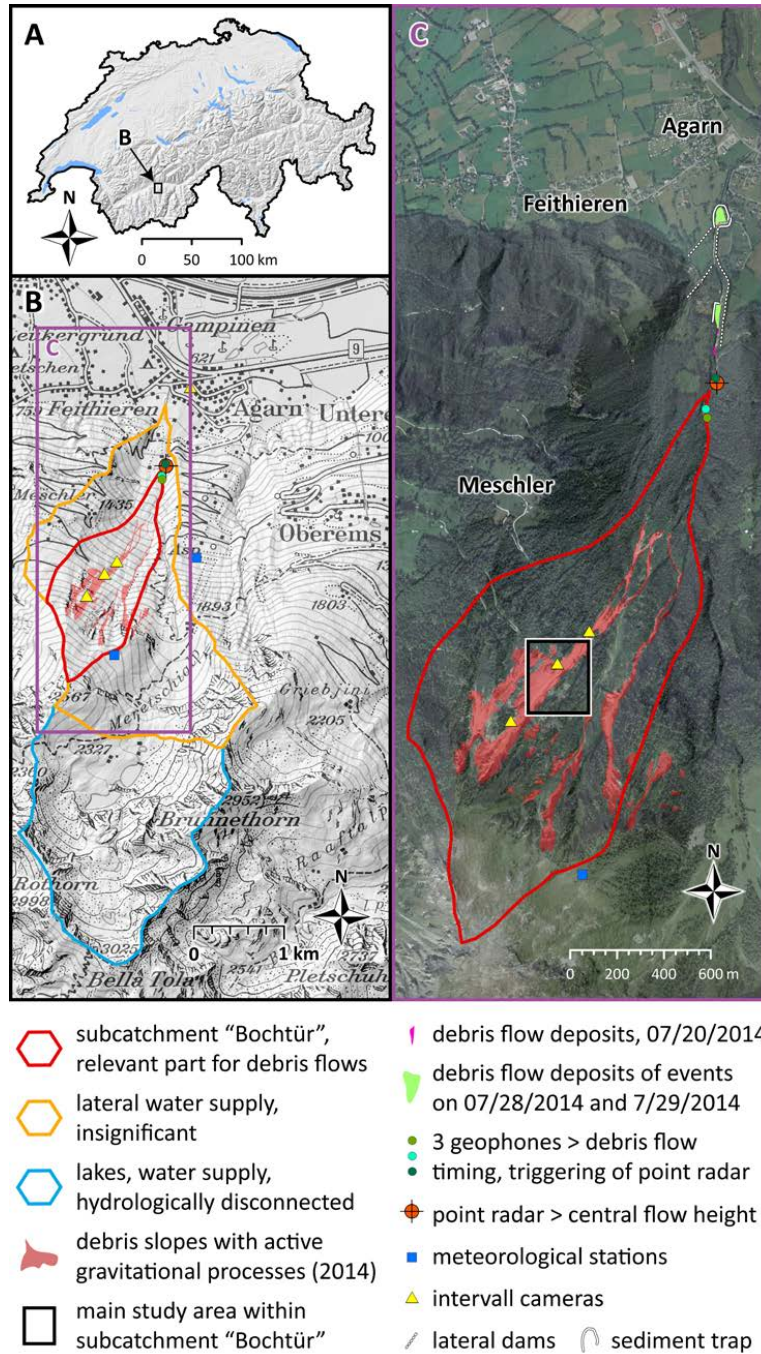
- 553 Godt, Jonathan W. and Coe, Jeffrey A.: Alpine debris flows triggered by a 28 July 1999  
554 thunderstorm in the central Front Range, Colorado, *Geomorphology*, Volume 84, Issues 1–2,  
555 Pages 80-97, ISSN 0169-555X, <http://dx.doi.org/10.1016/j.geomorph.2006.07.009>. 15 February  
556 2007.
- 557 Guthrie, R. H., Hockin, A., Colquhoun, L., Nagy, T., Evans, S.G. and Ayles, C.: An examination  
558 of controls on debris flow mobility: Evidence from coastal British Columbia. *Geomorphology*  
559 114, 601-613, 2010.
- 560 Han, Zheng; Chen, Guangqi; Li, Yange; Tang, Chuan; Xu, Linrong; He, Yi; Huang, Xun; Wang,  
561 Wei: Numerical simulation of debris-flow behavior incorporating a dynamic method for  
562 estimating the entrainment, *Engineering Geology*, Volume 190, Pages 52-64, ISSN 0013-7952,  
563 14 May 2015, available at: <http://dx.doi.org/10.1016/j.enggeo.2015.02.009> (last access: 10  
564 February 2016), 2015.
- 565 Hohermuth, B. and Graf, C.: Einsatz numerischer Murgangsimulationen am Beispiel des integralen  
566 Schutzkonzepts Plattenbach Vitznau. *Wasser Energ. Luft* 106, 4: 285-290, available at:  
567 <http://www.wsl.ch/wsl/info/mitarbeitende/grafc/pdf/14138.pdf> (last access: 10 February 2016),  
568 2014.
- 569 Hungr, O., McDougall, S. and Bovis, M.: Entrainment of material by debris flows, in *Debris-Flow*  
570 *Hazards and Related Phenomena*, edited by M. Jakob and O. Hungr, pp. 135-158, Springer,  
571 New York, 2005.
- 572 Hungr, O., Morgan, G. C. and Kellerhals, R.: Quantitative analysis of debris torrent hazards for  
573 design of remedial measures, *Can. Geotech. J.*, 21(4), 663-677, 1984.
- 574 Hungr, O. and McDougall, S.: Two numerical models for landslide dynamic analysis, *Comput.*  
575 *Geosci.*, 5, 978-992, 2009.
- 576 Hussin, H. Y., Quan Luna, B., van Westen, C. J., Christen, M., Malet, J.-P., and van Asch, Th. W.  
577 J.: Parameterization of a numerical 2-D debris flow model with entrainment: a case study of the  
578 Faucon catchment, Southern French Alps, *Nat. Hazards Earth Syst. Sci.*, 12, 3075-3090,  
579 doi:10.5194/nhess-12-3075-2012, 2012.
- 580 Iverson, R. M.: *The Physics of Debris Flows*: IN: *Reviews of Geophysics*, 35, 3, August 1997, p.  
581 245-296, published by Geophysical Union, Paper # 97RG00426, 1997.
- 582 Iverson, R.M., Reid, M.E., Logan, M., LaHusen, R.G., Godt, J.W. and Griswold, J.G.: Positive  
583 feedback and momentum growth during debris-flow entrainment of wet bed sediment. *Nature*  
584 *Geoscience* v. 4, no. 2, p. 116-121. doi: 10.1038/NGEO1040, 2011.
- 585 Iverson, R.M., Reid, M.E., Logan, M., LaHusen, R.G., Godt, J.W., and Griswold, J.G.: Positive  
586 feedback and momentum growth during debris-flow entrainment of wet bed sediment. *Nature*  
587 *Geoscience* v. 4, no. 2, p. 116-121. doi: 10.1038/NGEO1040, 2011.
- 588 May, C. L.: Debris flows through different forest age classes in the Central Oregon Coast Range, J.  
589 *Am. Water Resour. Assoc.*, 38(4), 1097-1113, 2002.



- 590 McCoy, S. W., Kean, J. W., Coe, J. A., Tucker, G. E., Staley, D. M. and Wasklewicz, T. A.:  
591 Sediment entrainment by debris flows: In situ measurements from the headwaters of a steep  
592 catchment, *J. Geophys. Res.*, 117, F03016, doi:10.1029/2011JF002278, 2012.
- 593 Medina, V., Hürlimann, M., and Bateman, A.: Application of FLATModel a 2-D finite volume  
594 code, to debris flows in the northeastern part of the Iberian Peninsula, *Landslides*, 5, 127–142,  
595 2008.
- 596 Meyer, G. A., and Wells, S. G.: Fire-related sedimentation events on alluvial fans, Yellowstone  
597 National Park, USA, *J. Sediment. Res.*, 67(5), 776–791, 1997.
- 598 Oggier, N. and McArdell, B. W.: Ereignisanalyse - Murgangereignisse Meretschibach 20./28./29.  
599 Juli 2014. Birmensdorf, 21. Januar 2015, (only available in German), 2015a.
- 600 Oggier, N. and Bösch, R.: Zwischenbericht, Drohnenflug Meretschibach 28. Oktober 2014,  
601 Birmensdorf, 26. Februar 2015, (only available in German), 2015b.
- 602 Pierson, T. C., Janda, R. J., Thouret, J.-C. and Borrero, C. A.: Perturbation and melting of snow and  
603 ice by the 13 November 1985 eruption of Nevado del Ruiz, Colombia, and consequent  
604 mobilization, flow and deposition of lahars. *J. Volcanol. Geotherm. Res.* 41, 17–66, 1990.
- 605 Prancevic, J. P., and Lamb, M. P.: Particle friction angles in steep mountain channels, *J. Geophys.*  
606 *Res. Earth Surf.*, 120, doi:10.1002/2014JF003286, 2015a.
- 607 Prancevic, J. P., and M. P. Lamb: Unraveling bed slope from relative roughness in initial sediment  
608 motion, *J. Geophys. Res. Earth Surf.*, 120, doi:10.1002/2014JF003323, 2015b.
- 609 Procter, J., Cronin, S. J., Fuller, I. C., Lube, G. and Manville, V.: Quantifying the geomorphic  
610 impacts of a lake-breakout lahar, Mount Ruapehu, New Zealand, *Geology*, 38(1), 67–70, 2010.
- 611 Revellino, P., Hungr, O., Guadagno, F. M. and Evans, S. G.: Velocity and runout simulation of  
612 destructive debris flows and debris avalanches in pyroclastic deposits, Campania region, Italy,  
613 *Environ. Geol.*, 45(3), 295–311, 2004.
- 614 Scheingross, J. S., Winchell, E. W., Lamb, M. P. and Dietrich, W. E.: Influence of bed patchiness,  
615 slope, grain hiding, and form drag on gravel mobilization in very steep streams, *J. Geophys.*  
616 *Res. Earth Surf.*, 118, 982–1001, doi:10.1002/jgrf.20067, 2013.
- 617 Scheuner, T., Keusen, H., McArdell, B. W., and Huggel, C.: Murgangmodellierung mit dynamisch-  
618 physikalischem und GIS-basiertem Fliessmodell, Fallbeispiel Rotlauigraben, Guttannen, August  
619 2005, *Wasser Energie Luft*, 101: 15–21 (only available in German), 2009.
- 620 Scheuner, T., Schwab, S., and McArdell, B. W.: Application of a two-dimensional numerical  
621 model in risk and hazard assessment in Switzerland, in 5<sup>th</sup> DFHM, Padua, Italy, 2011.
- 622 Schürch, P., Densmore, A. L., Rosser, N. J., and McArdell, B. W.: Dynamic controls on erosion  
623 and deposition on debris-flow fans, *Geology*, 39, 827–830, 2011.
- 624 Scott, K. M., Vallance, J. W., Kerle, N., Macias, J. L. Strauch, W. and Devoli, G.: Catastrophic  
625 precipitation-triggered lahar at Casita volcano, Nicaragua: Occurrence, bulking and  
626 transformation, *Earth Surf. Processes Landforms*, 30(1), 59–79, doi:10.1002/esp.1127, 2005.



- 627 Suwa, H., and Okuda, S.: Dissection of valleys by debris flow, *Z. Geomorphology*, 35, 164-182,  
628 1980.
- 629 Szymczak, S., Bollschweiler, M., Stoffel, M. and Dikau, R.: Debris-flow activity and snow  
630 avalanches in a steep watershed of Valais Alps (Switzerland): Dendrogeomorphic event  
631 reconstruction and identification of triggers. *Geomorphology* 116, 107-114, 2010.
- 632 Tobler, D., Kull, I., Jacquemart, M., and Haehlen, N.: Hazard Management in a Debris Flow  
633 Affected Area: Case Study from Spreitgraben, Switzerland, *Landslide Science for a Safer  
634 Geoenvironment*, 3, 25–30, doi:10.1007/978-3-319-04996-0\_5, 2014.
- 635 Vallance, J. W. and Scott, K. M.: The Osceola Mudflow from Mount Rainier: Sedimentology and  
636 hazard implications of a huge clay-rich debris flow, *Geol. Soc. Am. Bull.*, 109(2), 143-163,  
637 1997.
- 638 Vandine, D.F. and Bovis M.: History and goals of Canadian debris-flow research, a review. *Nat  
639 Hazards* 26:69–82, 2002.
- 640 Wang, G., Sassa, K. and Fukuoka, H.: Downslope volume enlargement of a debris slide\_debris  
641 flow in the 1999 Hiroshima, Japan, rainstorm. *Eng. Geol.* 69, 309-330, 2003.

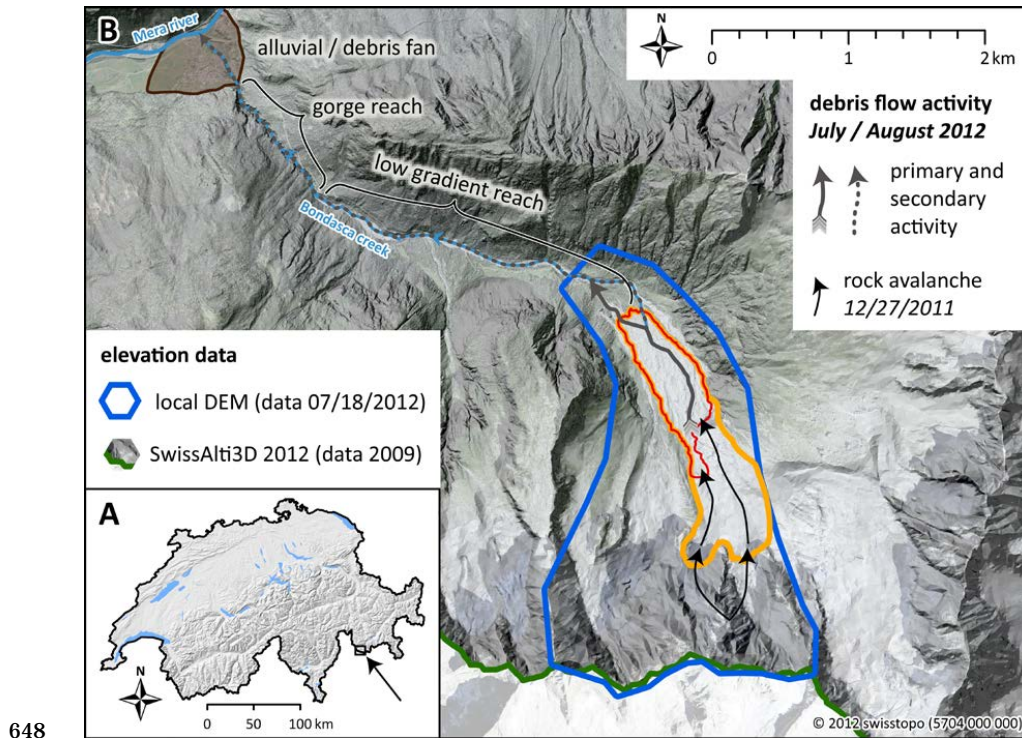


642

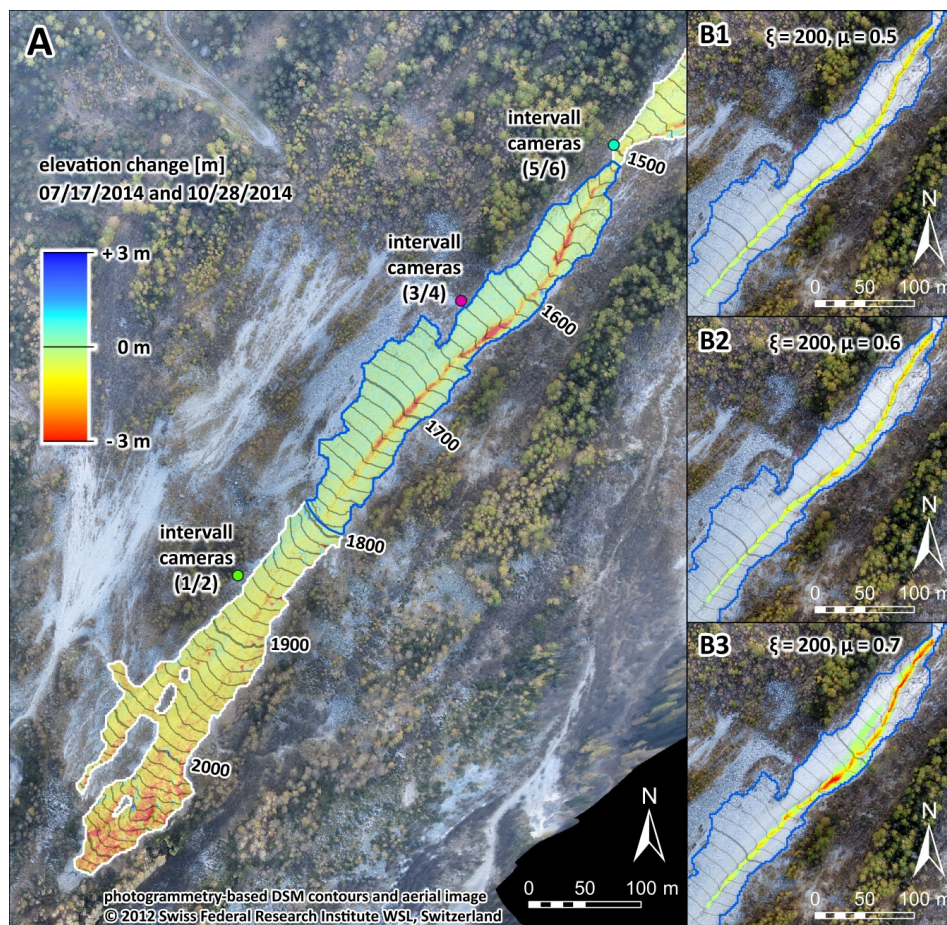
643 **Figure 1.** **A.** Location of the Meretschibach catchment in Southern Switzerland. **B.** Subcatchments  
 644 of the Meretschibach and locations of the instrumentation site and data available for the erosion  
 645 model analyses **C.** Initiation zone of the July 2014 events and camera positions. The main study



646 channel reach for the model testing is located in the middle part of “Bochtür” (black-white  
647 retangle), swissimage©2014, swisstopo (5704 000 000) (2014).

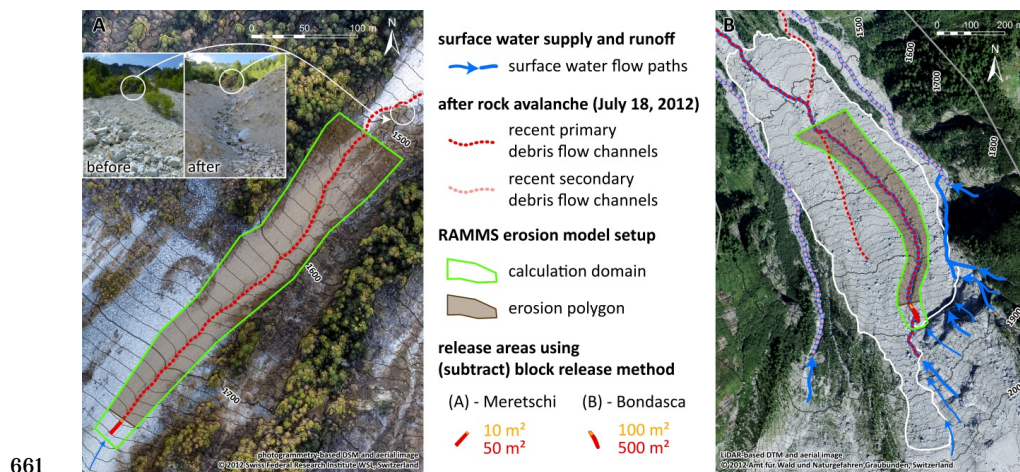


649 **Figure 2.** A. Location of the Bondasca catchment in south-eastern Switzerland close to the border  
650 to Italy. B. Perimeter of the 27 December 2011 rock avalanche deposit, including the main  
651 deposition area (yellow polygon) and the deposits lower-elevation deposits which have been  
652 partially exposed to erosion by debris flows in 2012 (red polygon). The 2012 post-event digital  
653 elevation model (lidar, blue polygon) is from 18 July 2012 (data courtesy of the Amt für Wald,  
654 Canton Graubünden). Pre-event digital elevation model (lidar) for 2009 is from the SwissAlti3D  
655 (version 2012) data set from swisstopo, ©2012, swisstopo (5704 000 000) . The grey solid arrow  
656 indicates the main debris-flow channel formed in 2012.

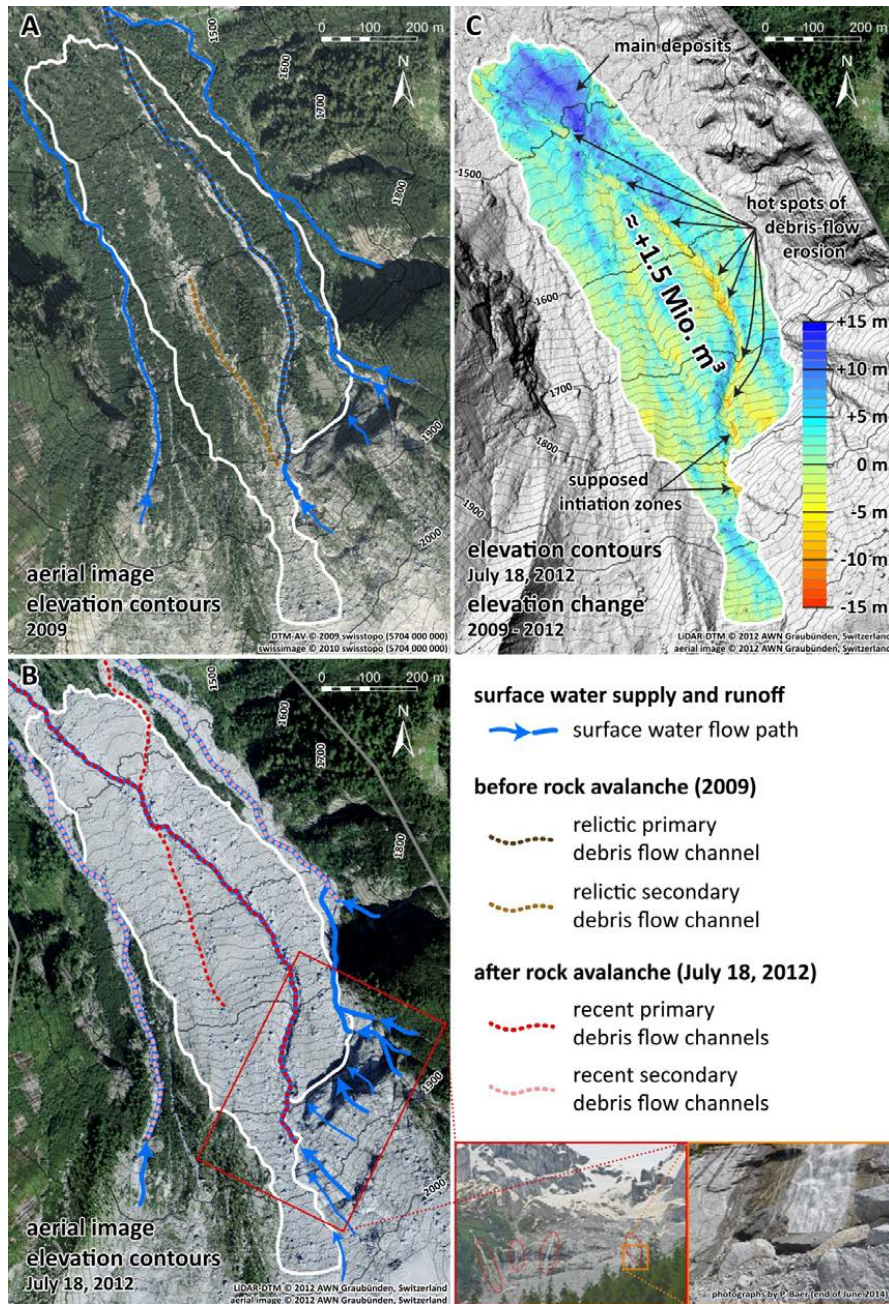


657

658 **Figure 3.** Calibration of modelled erosion patterns (**B1 to B3**) to the observed erosion depths (**A**) in  
659 the upper open debris slopes of the “Bochtür” catchment (Meretschibach) by varying values for the  
660 friction parameter  $\mu$ . The blue polygon demarks the area where a differential DTM is available.

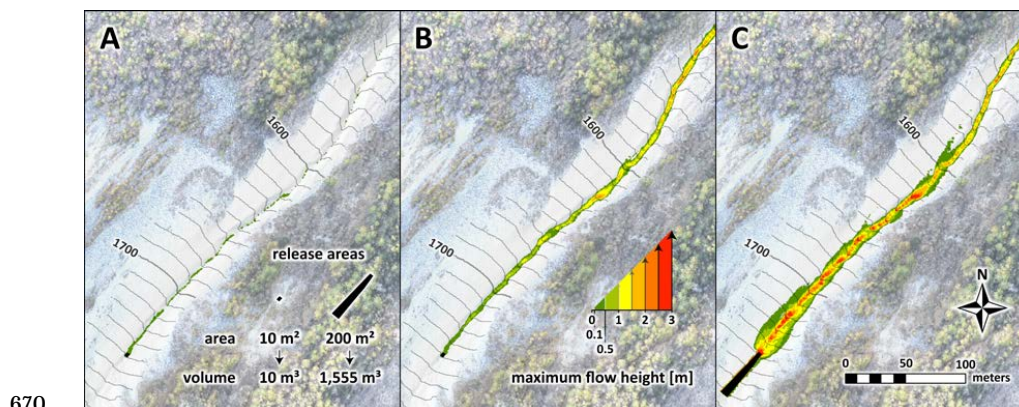




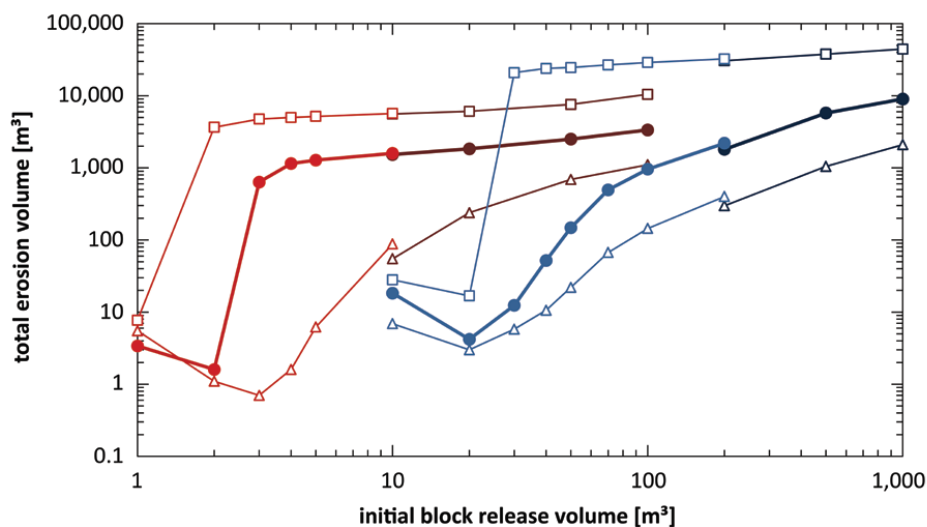


665

666 **Figure 5.** Overview of rock avalanche deposits, subsequently formed debris flow channels, and the  
 667 resulting overall elevation change in the Bondasca catchment (A, B). The elevation change map  
 668 2009 to 2012 (C) includes both the rock avalanche ( $\approx 1.5 \text{ Mio m}^3$  on 27 Dec. 2011) and the first  
 669 two debris flow events (5 and 14 July 2012).



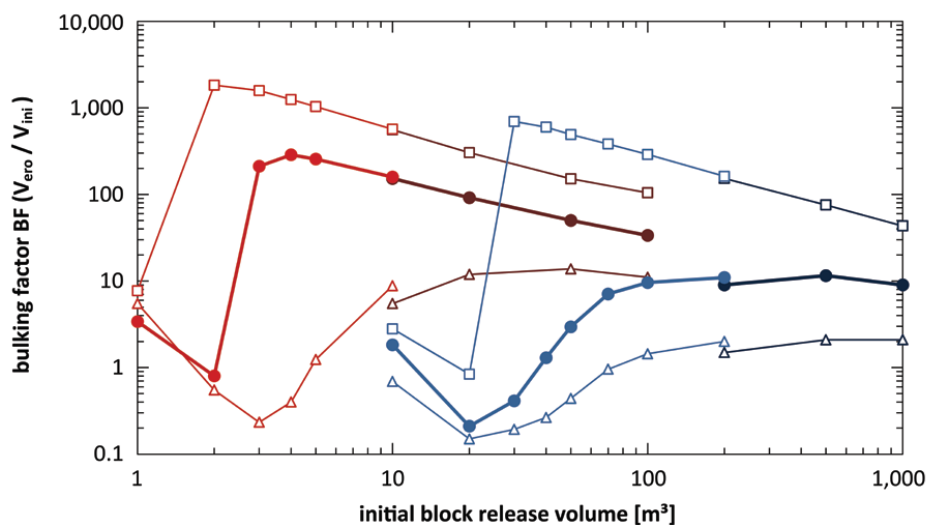
671 **Figure 6.** Comparison of runout patterns at “Bochtür” in the Meretschi catchment. The debris flow  
672 modeling is conducted using a (subtract) block release volume of (A) 10 m<sup>3</sup> and no-entrainment  
673 modeling, of (B) 10 m<sup>3</sup> and entrainment modeling as well as a total (subtract) block release volume  
674 of (C) 1,555 m<sup>3</sup> (sum of release and eroded volume from (B)) and no-entrainment modeling.



|                                       | Meretschi  | Bondasca   |
|---------------------------------------|--|--|
| calibrated parameters                 | $\xi = 200 \text{ m}^2\text{s}^{-1}, \mu = 0.60$       | $\xi = 400 \text{ m}^2\text{s}^{-1}, \mu = 0.30$ |
| release areas                         | — 10 m <sup>2</sup> — 50 m <sup>2</sup>                | — 100 m <sup>2</sup> — 500 m <sup>2</sup>        |
| erosion rates<br>(Frank et al., 2015) | —△— 1.25 cm s <sup>-1</sup> —●— 2.5 cm s <sup>-1</sup> | —□— 5.0 cm s <sup>-1</sup>                       |

675

676 **Figure 7.** Sensitivity of modeled erosion volume to initial block release volume in the  
 677 Meretschibach and in the Bondasca catchments.



|                                       | Meretschi  | Bondasca   |
|---------------------------------------|--|--|
| calibrated parameters                 | $\xi = 200 \text{ m}^2 \text{ s}^{-1}, \mu = 0.60$     | $\xi = 400 \text{ m}^2 \text{ s}^{-1}, \mu = 0.30$ |
| release areas                         | — 10 m <sup>2</sup> — 50 m <sup>2</sup>                | — 100 m <sup>2</sup> — 500 m <sup>2</sup>          |
| erosion rates<br>(Frank et al., 2015) | —△— 1.25 cm s <sup>-1</sup> —●— 2.5 cm s <sup>-1</sup> | —□— 5.0 cm s <sup>-1</sup>                         |

678

679 **Figure 8.** The bulking factor  $BF = V_{\text{ero}}/V_{\text{ini}}$  of the modeled total erosion volume  $V_{\text{ero}} [\text{m}^3]$  to initial  
 680 block release volume  $V_{\text{ini}} [\text{m}^3]$  in the Meretschibach and Bondasca catchments.